

DesignCon 2006

Slow-Wave Causal Model for Multi Layer Ceramic Capacitors

Istvan Novak
Gustavo Blando
Jason R. Miller

Sun Microsystems, Inc.
Tel: (781) 442 0340, e-mail: istvan.novak@sun.com



Abstract

There is an ongoing interest in refining the simulation models for passive components in electronic circuits. For simple analyses, bypass capacitors are modeled by a series C-R-L equivalent network. To capture the frequency dependency of the circuit parameters, more complex equivalent circuits can be used: ladder L-R networks to model the frequency dependent inductance and resistance and/or C-R networks to model the frequency dependent capacitance. These equivalent circuits have the advantage of being compatible with both time-domain and frequency domain SPICE simulations, but the optimum topology of the equivalent circuit may depend on the type and construction of capacitor. This paper first summarizes the current distributions inside MLCC parts simulated with a bedspring model and we make some counter-intuitive observations about the frequency dependency of inductance and resistance in tall MLCC parts. Based on those observations we then derive a slow-wave causal model, which represents the capacitor with a periodically loaded lossy transmission line. It is shown that the load circuit in the unit cell corresponds to the waveguide formed by two adjacent capacitor plates. The unit cells are further simplified and lumped together into one lossy, open-ended transmission line with a series R-L circuit capturing the impedance of the cover layer of the capacitor. The parameters of the single lossy transmission line are derived from the geometry and material properties. It is shown that the counter-intuitive features in the model are captured by a virtual capacitance and dielectric loss tangent, which combine the dielectric loss of the ceramic and the resistive losses of the capacitor plates. The model is shown to capture the important characteristics of measured data, and it is simple enough to be used in multiple copies in circuit simulators.

Author Biographies

Istvan Novak is signal-integrity senior staff engineer at SUN Microsystems, Inc. Besides signal-integrity design of high-speed serial and parallel buses, he is engaged in the design and characterization of power-distribution networks and packages for mid-range servers. He creates simulation models, and develops measurement techniques for power distribution. Istvan has twenty plus years of experience with high-speed digital, RF, and analog circuit and system design. He is Fellow of IEEE for his contributions to signal-integrity and RF measurement and simulation methodologies.

Gustavo Blando is a signal Integrity engineer with over 10 years of experience in the industry. Currently at Sun Microsystems he is responsible for the development of new processes and methodologies in the areas of broadband measurement, high speed modeling and system simulations. He received his M.S. from Northeastern University.

Jason Miller is currently a Staff Engineer at Sun Microsystems where he works on ASIC development, ASIC packaging, interconnect modeling and characterization, and system simulation. He received his Ph.D. in Electrical Engineering from Columbia University.

I. Introduction: Present modeling options

When considering the parasitics of bypass capacitors, a widely used simple model is a series C-R-L network, where C is the capacitance of the part, R is the Equivalent Series Resistance (ESR) and L is the Equivalent Series Inductance (ESL), as shown in Figure 1. In its simple form, C, ESR and ESL are assumed to be frequency independent constants. However, measured data indicates [1] that all three of these parameters are eventually frequency dependent and furthermore may be inter-related through the application geometry.

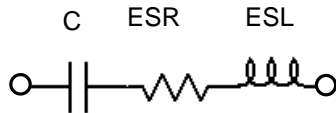


Figure 1. Simple RLC equivalent circuit of a capacitor.

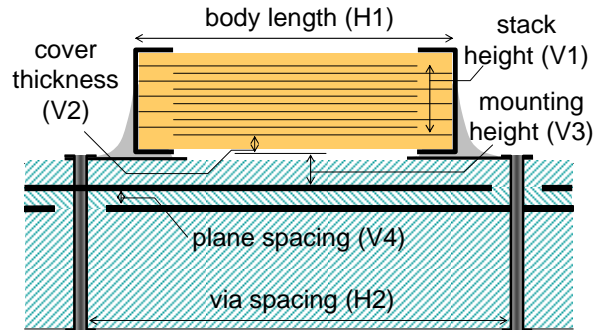


Figure 2. Vertical cross section of an MLCC mounted to PCB planes.

The capacitance may be frequency dependent, primarily because of dielectric losses [2].

ESR is the result of transforming the parallel dielectric losses and series conductive losses into a single series resistance value. As long as tangent delta of the dielectric material varies little with frequency, the parallel loss resistance drops inversely with frequency. The series resistance of the part comes from the terminals and conductive layers on the dielectric sheet(s). Apart from bulk capacitor constructions, like tantalum brick capacitors and alike, the capacitor plates in high-CV MLCCs are thin enough that in the frequency range of interest their thickness is less than the skin depth, and therefore the AC resistance contributions of the plates themselves do not vary much with frequency. Overall ESR still varies at high frequencies, due to non-uniform current distribution in the plates [4]

Inductance depends both on the internal construction of the part and the external geometry forming the closed current loop. As illustrated in Figure 3 for the case of a reverse-geometry Multi-Layer Ceramic Capacitor (MLCC) attached to a pair of planes on a PCB, the measured impedance of the part exhibits strong frequency dependency on all three of the parameters.

When extracting capacitor parameters from measured data, we face a further complication: ESR is simply the real part of the measured impedance (after the proper calibration and/or deembedding process), but the capacitive and inductive reactances show up in a superimposed way in the imaginary part of the measured impedance. If capacitance and inductance were frequency independent, extracting them from the imaginary part of measured impedance would be easy. Because the capacitive and inductive reactances change with frequency in the opposite way, we know that at frequencies much below the Series Resonance Frequency (SRF) the inductive reactance is negligible and from the measured reactance we can calculate the capacitance. Similarly from a measured reactance value at a frequency much above SRF we could calculate the inductance. This approach is assumed for instance in [3] and [4]. With relatively strong frequency dependency of capacitance and/or inductance, which is the case of tall capacitor stacks with lossy dielectrics and aggressive mounting, using a low-frequency

capacitance and a high-frequency inductance can not uniquely resolve the frequency dependent capacitance and inductance values around SRF. One step further is to iteratively approximate the capacitance and inductance close to SRF and use those (constant) values to extract the frequency dependent capacitance and inductance curves [5]. This improves accuracy and the range of validity for the extracted capacitance and inductance curves, but unless we have further data points or constraints, we still cannot uniquely resolve the two unknowns, $C(f)$ and $ESL(f)$, from one data point of $Im\{Z(f)\}$.

Instead of trying to blindly extract the parameters from measured data, more sophisticated equivalent circuits can also be used to fit the measured data on the model. Equivalent circuits composed of frequency independent resistors, capacitors and inductors unconditionally guarantee causality and easy compatibility to circuit simulators. To describe frequency dependent capacitance and ESR of bulk capacitors, [6] suggests a composite RLC network. To capture the frequency dependent ESR and ESL of MLCCs, [7] uses a resonant ladder network, while [8] proposes a transmission-line model.

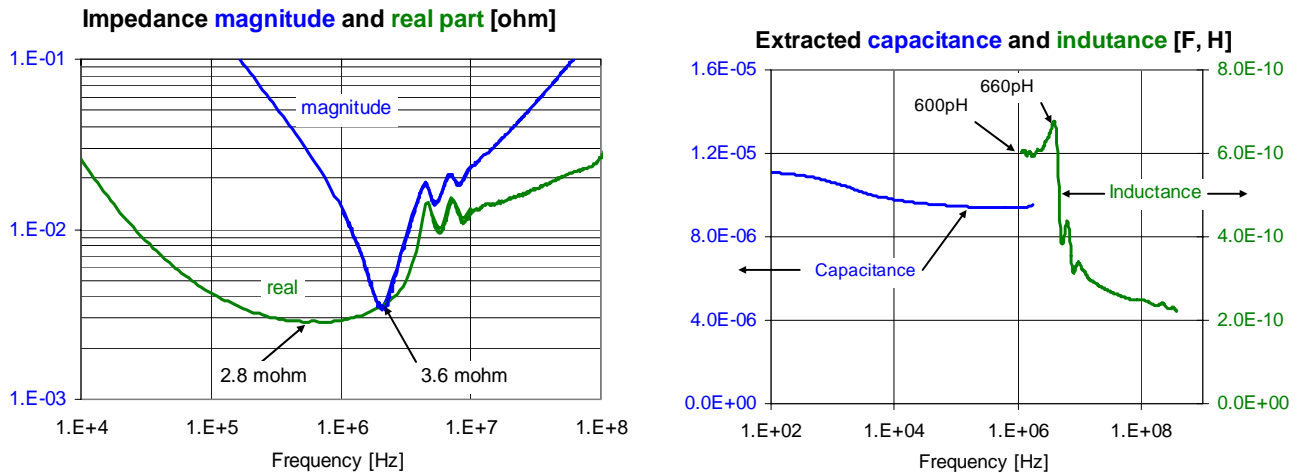


Figure 3. Measured impedance magnitude of a 10uF 0508 MLCC with the real part of the impedance (on the left), and extracted capacitance and inductance versus frequency (on the right).

For MLCC parts, it is customary to assume that the capacitive and inductive currents balance themselves at SRF and therefore at that frequency the current uniformly penetrates all plates and for this reason the lowest ESR value occurs at SRF. Similarly, it is usually assumed that inductance monotonically drops from its low-frequency value towards the high-frequency loop inductance.

In contrast to usual expectations, data on Figure 3 indicates that the minimum of the impedance real part is not at SRF: at 600kHz ESR is 2.8 milliohms; whereas at the 2.1MHz SRF the ESR reading is 3.6 milliohms. Moreover, the $ESL(f)$ value extracted according to the procedure in [5] results in 600pH at SRF, but the inductance first increases with frequency, instead of decreasing, reaching a 660pH peak at 4.2MHz before it starts going down. Is this due to measurement errors or a deficiency in the extraction procedure, or really ESR and ESL behave contrary to common assumptions? As it was shown in detail in [9], this counter intuitive behavior comes from the vertical resonances (and at higher frequencies, to a lesser degree, from horizontal resonances) along the capacitor body. These features can be captured by using a two-dimensional transmission-line or RLGC bedspring array.

Figure 4 shows the partial schematics of the bedspring model, where the capacitor plates are grouped into ten horizontal layers, each layer broken down into ten segments. Note that the grid size of ten by ten is somewhat arbitrary, but proved to be sufficient to capture the major features.

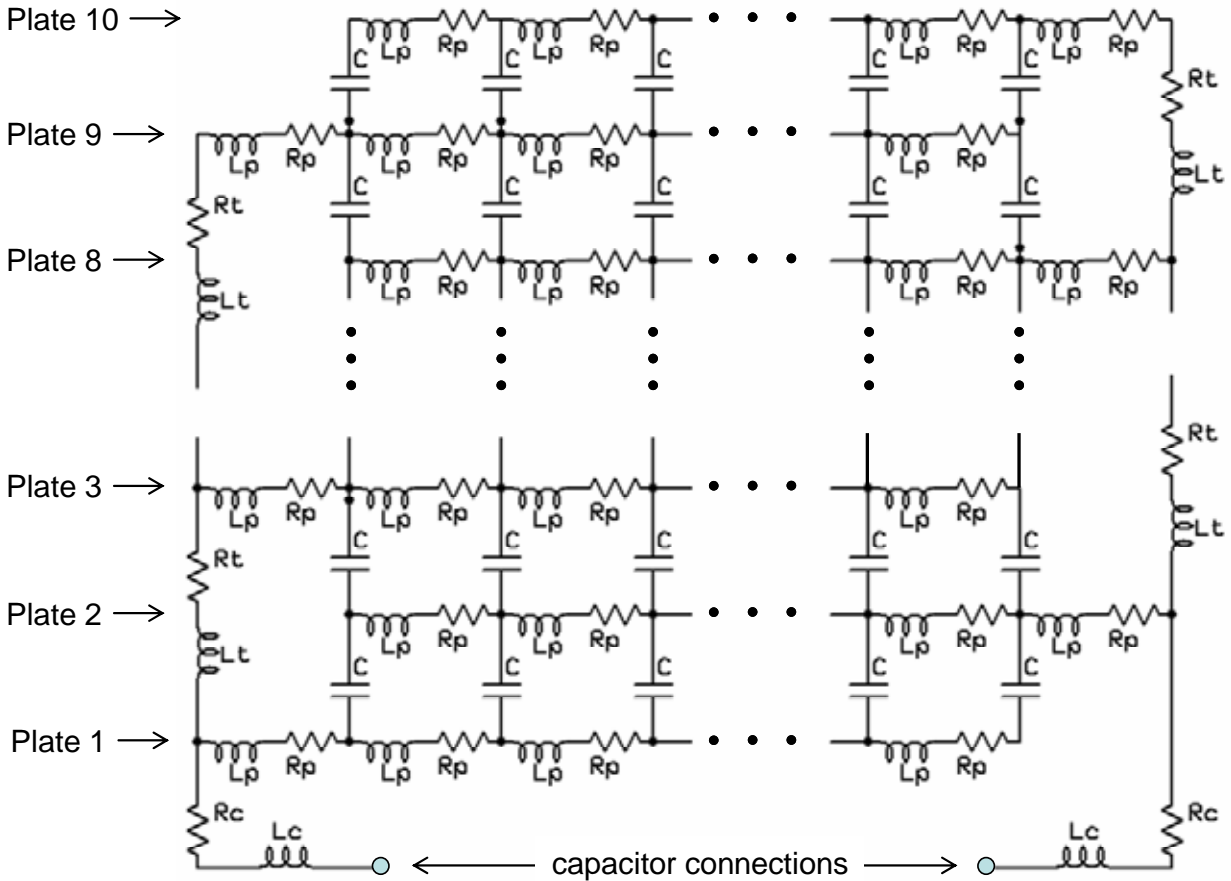


Figure 4. Partial schematics of the bedspring capacitor model. The model consists of ten capacitor plates, 1 through 10. The lowest capacitor plate, connecting to the PCB, is Plate 1. Plates 1, 3, 5, 7 and 9 are connected to the left terminal. Plates 2, 4, 6, 8 and 10 are connected to the right terminal. Each capacitor plate is divided into ten equal segments (plus an end piece), represented by series RL networks. At each internal plate node, a capacitor represents the dielectrics.

Figure 5 shows the impedance magnitude and real part of impedance simulated at the connection terminals. The schematics entries used for the simulation are listed to the right of the chart. Note that the bedspring model captures all of the important features that we want to study: it shows that impedance real part starts to increase below SRF, and there is a set of dampened, but pronounced secondary resonances. Because we assume no dielectric loss, the impedance real part at low frequencies does not rise. The current-distribution plots in [9] showed also the reason why the inductance starts to rise around SRF before it eventually goes down. For a fully animated illustration of currents in the capacitor plates and in the dielectrics, see [10]. Here we reproduce the current distribution plots only at SRF. On the left chart of Figure 6 we see the current distribution along the capacitor plates, whereas on the right-hand plot the current distribution in the dielectric layers is shown. The nonlinear current distribution is a clear indication that both ESR and ESL are increased.

While the bedspring model is unconditionally causal, and it is useful to study the vertical and horizontal resonances in MLCC parts, the model is clearly too complicated to be used in PDN simulations, where we may need dozens or hundreds of such capacitor models in the same network.

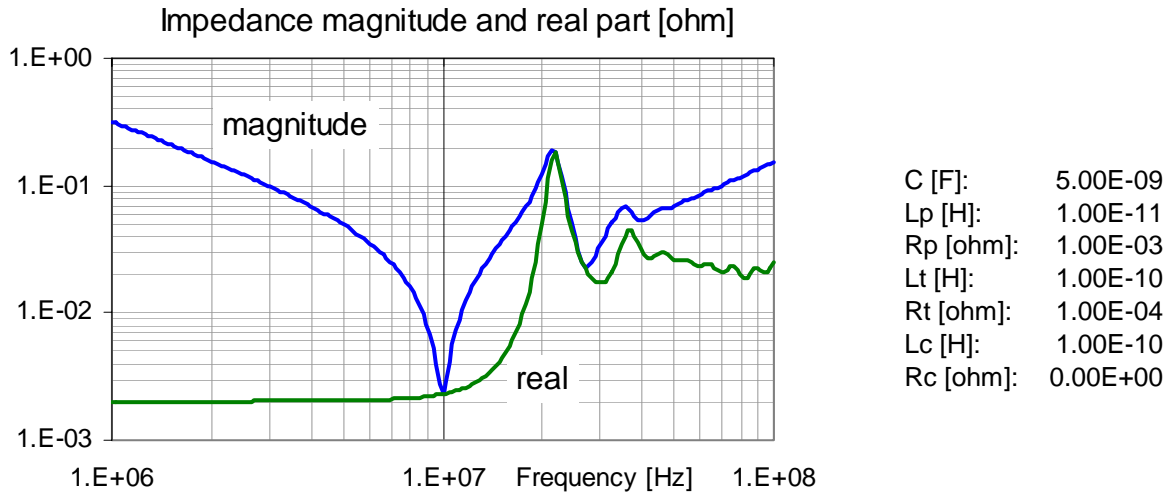


Figure 5. Simulated impedance magnitude and impedance real part at the capacitor connections terminals of the circuit shown in Figure 4. Circuit parameter values are shown in the table on the right.

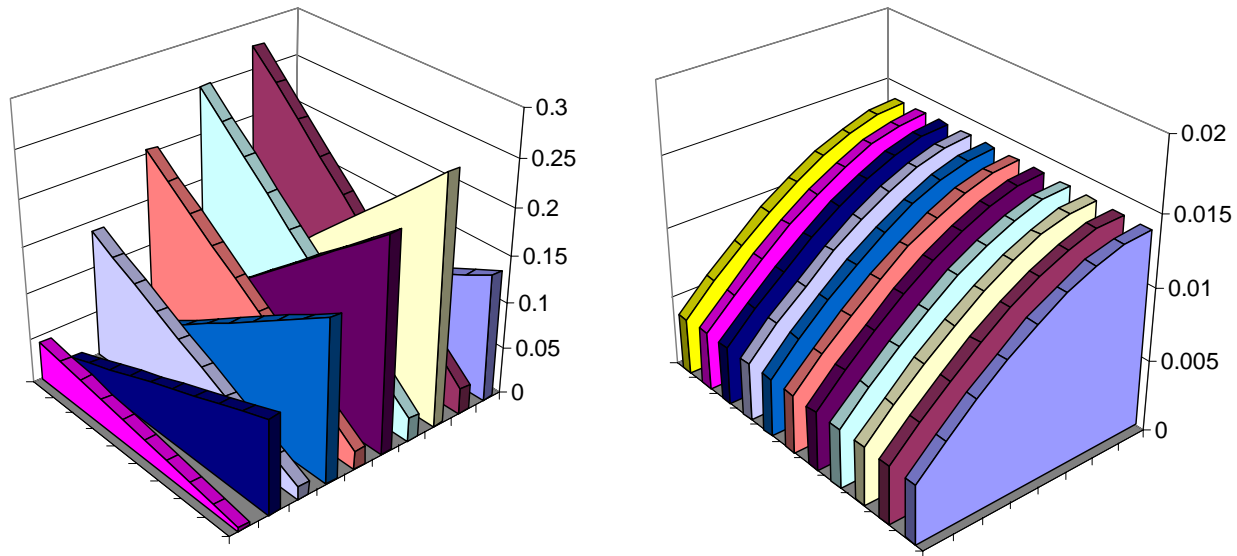


Figure 6. Current distribution along the capacitor plates (on the left) and inside the dielectrics (on the right) at the 10MHz SRF. Vertical axis unit: A.

The black-box behavioral model introduced in [9] offers a unified model for bypass capacitors, simple enough to use many of them in frequency-domain PDN simulations. The model uses only three components, a series C-R-L circuit, but all three elements are frequency dependent. The frequency dependency of each element is captured and described by seven parameters, resulting in a total of 21 parameters for one model. The expressions capturing the frequency dependencies are based on the behavior of measured capacitor pieces. The parameters can be obtained either by manual or by semi-automatic curve fitting. However, the black-box model does not guarantee causal behavior, and because the three components are frequency dependent, it is not well suited for time-domain simulations.

II. Slow-wave causal model

The unit-cell model

The slow-wave causal model is built on the realization that a multi-layer ceramic capacitor is a periodically loaded lossy transmission line. The unloaded transmission line is formed by the two vertical terminals of the capacitor, by removing the capacitor plates, but leaving the dielectric material in place. This vertically oriented unloaded transmission line in itself is already lossy: the terminals have finite resistance, and the dielectric material has finite dielectric loss tangent. It is also known that causality dictates capacitance to change with the log of frequency in proportion to the dielectric loss tangent. In an MLCC part, the large capacitance is achieved by inter digitated capacitor plates, attached alternating to the opposite terminals. These capacitor plates form a set of periodically arranged lossy transmission lines, attached orthogonally to the capacitor terminals. As it will be shown, the multitude of capacitor plates will not only increase the total capacitance of the part, but it also behaves like a dielectric material with increased loss tangent and additional frequency dependency of capacitance. The virtual loss tangent is a mix of the loss tangent of the original dielectric material and the resistive loss of the capacitor plates.

The expectation is that if we properly assign the dimensions and material constants, or if we do a blind optimization of these parameters to match the measured behavior of a capacitor, all of the major features will be captured simultaneously, without the need to change and optimize independently capacitance, resistance and inductance values (which was the case in [9]). Also, the model is based on the physical properties of the structure, and it guarantees that the model will be causal.

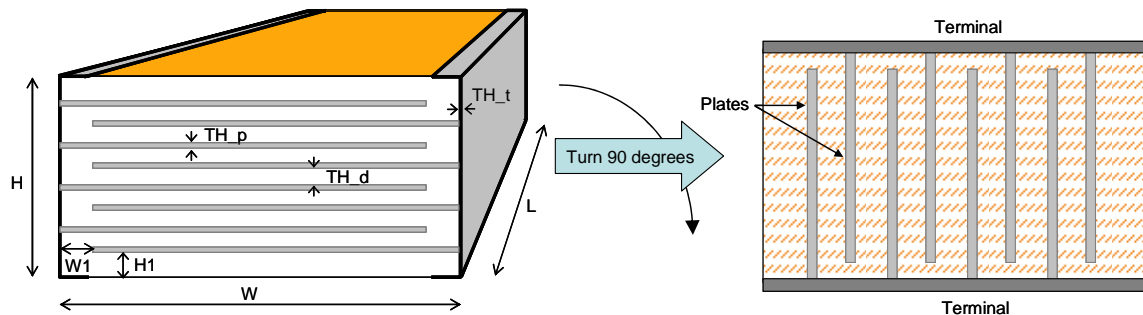


Figure 7. Left: side view of MLCC with the important dimensions. Right: representation of the same MLCC by turning it 90 degrees.

The sketch on the left side of Figure 7 defines the major dimensions of an MLCC, relevant to our calculations. We assume that the rectangular capacitor body is W wide, L long and H high. The illustration here shows a reverse-geometry capacitor, because for the correlation we will use the measured data on the previous 10 μ F 0508 MLCC example. The calculations and methodology, however, do not mandate a reverse-geometry capacitor. For other geometries, such as regular or inter-digitated capacitors, L , W and H can be changed appropriately as needed.

To somewhat simplify the calculations, the capacitor cross section is assumed to be symmetrical, both horizontally and vertically. We assume the same $H1$ cover thickness both on top and bottom. A similar horizontal symmetry assumes that capacitor plates are stopping $W1$ distance from the unconnected

terminals at both sides. This symmetry is assumed here only for sake of convenience; the procedure can be easily extended to different top and bottom cover thicknesses and/or for different end gaps at the left and right terminals.

The capacitor plate thickness is TH_p, each dielectric layer between the plates is TH_d thick. The vertical capacitor terminals are assumed to be TH_t in thickness. We further assume that the dielectric material has ϵ_d dielectric constant and $\tan \delta$ loss tangent at a given working frequency, and their frequency dependent values are inter-related through the causal requirement [2]. The capacitor plates have a conductivity of σ_p , the terminal material has a conductivity of σ_t .

The periodically loaded transmission-line model becomes apparent when we turn the capacitor sideways and distort the aspect ratio. As shown on the right side of Figure 7, the height (H) of the original capacitor body becomes the length of the transmission line, and the capacitor plates will represent a periodical loading along the transmission line.

The capacitance of the unloaded transmission line equals the capacitance of the capacitor body between the vertical terminals, without the capacitor plates:

$$C_0 = \epsilon_0 \epsilon_d \frac{L * H}{W} \quad (1)$$

The propagation delay of the unloaded transmission line equals the propagation delay along the empty vertical capacitor body, with the capacitor plates removed but dielectric material in place:

$$t_{pd0} = \frac{H}{v} = H \sqrt{\epsilon_0 \epsilon_d \mu_0} \quad (2)$$

With C_0 and t_{pd0} known, we can calculate the characteristic impedance and the inductance of the unloaded vertical transmission line:

$$L_0 = \frac{t_{pd0}^2}{C_0} = \mu_0 \frac{H * W}{L} \quad \text{and} \quad Z_{00} = \sqrt{\frac{L_0}{C_0}} = \frac{120\pi W}{\sqrt{\epsilon_0} L} \quad (3)$$

The resistance of each terminal along its entire vertical length is:

$$R_t = \frac{1}{\sigma_t} \frac{H}{L * TH_t} \quad (4)$$

From (1) through (4), we can calculate the parameters of the two end pieces, simply by scaling the unloaded transmission line length by the ratio of H1/H for each end piece:

$$t_{pd_end} = t_{pd0} \frac{H1}{H} \quad (5)$$

The end-piece transmission lines are denoted by suffix *_end*.

As shown on the left of Figure 8, adjacent capacitor plates along the terminal will create the periodical loading. The impedance of the entire capacitor is observed at the left end of the transmission line; the x at the right end of the structure indicates that the right-hand side end of the structure is open.

The loading is created by the lossy, open-ended transmission lines formed by adjacent plates. Following (1) through (4), we can calculate the parameters of a transmission line formed by adjacent capacitor plates. This transmission line is denoted by suffix *-p*.

$$C_p = \epsilon_0 \epsilon_d L \frac{W - 2 * W1}{TH_d} \quad (6)$$

$$t_{pdp} = \frac{W - 2 * W1}{v} = (W - 2 * W1) * \sqrt{\epsilon_0 \epsilon_d \mu_0} \quad (7)$$

$$L_p = \frac{t_{pdp}^2}{C_p} = \mu_0 \frac{TH_d * (W - 2 * W1)}{L} \quad \text{and} \quad Z_{0p} = \sqrt{\frac{L_p}{C_p}} = \frac{120\pi TH_d}{\sqrt{\epsilon_0} L} \quad (8)$$

$$R_p = \frac{1}{\sigma_p} \frac{W - W1}{L * TH_p} \quad (9)$$

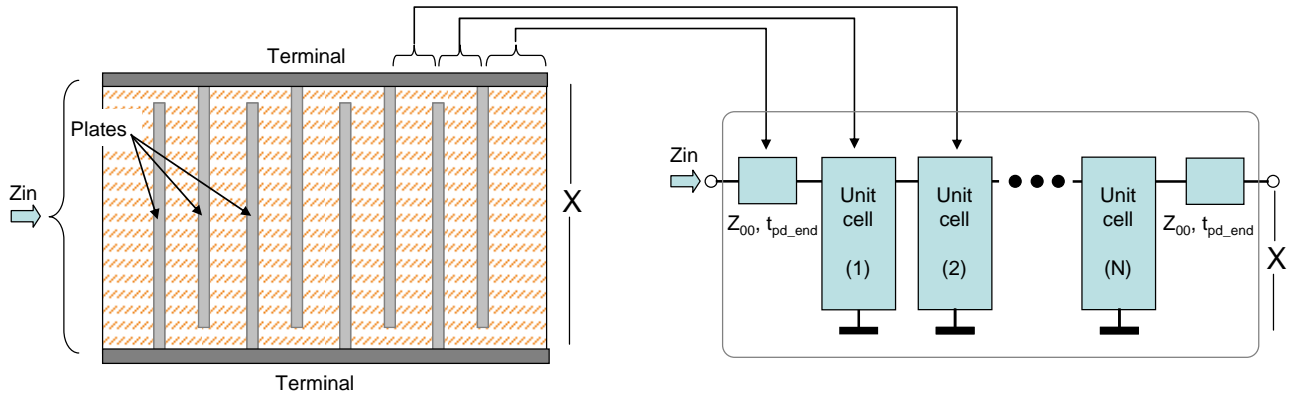


Figure 8. Slow-wave periodically loaded model of MLCC. The periodically loaded transmission line is broken down into symmetrical unit cells, each cell representing a length equal to the capacitor-plate pitch. The end pieces, corresponding to the bottom and top dielectric covers, are represented by unloaded transmission-line sections.

From N capacitor plates, we get $N-1$ pairs to create the periodical loading. For $N \gg 1$, we can approximate the number of cells in the periodically loaded structure with N .

The number of plates, the dielectric and plate thicknesses and the top/bottom cover thicknesses are inter-related through the following formula:

$$N = \frac{H - 2 * H1}{TH_p + TH_d} \quad (10)$$

The conductive and dielectric losses of the transmission lines are, in theory, frequency dependent. The skin depth in conductors is defined as:

$$skin_depth = \sqrt{\frac{1}{\pi f \sigma \mu}} \quad (11)$$

The skin depth in copper reaches $1\mu\text{m}$ at 1GHz frequency. To meet the requirements of the high ceramic firing temperature, capacitor plates use materials with conductivity lower than that of copper.

The lower conductivity increases the skin depth. This means the resistance of individual capacitor plates is skin-depth limited and is relatively frequency independent up to hundreds of MHz frequencies. The terminals are usually much thicker than the capacitor plates, and therefore their resistance and inductance may show somewhat more frequency dependency.

The dielectric losses are represented by a parallel conductance G in the transmission-line model:

$$G = 2\pi f C \tan_{\delta} \tag{12}$$

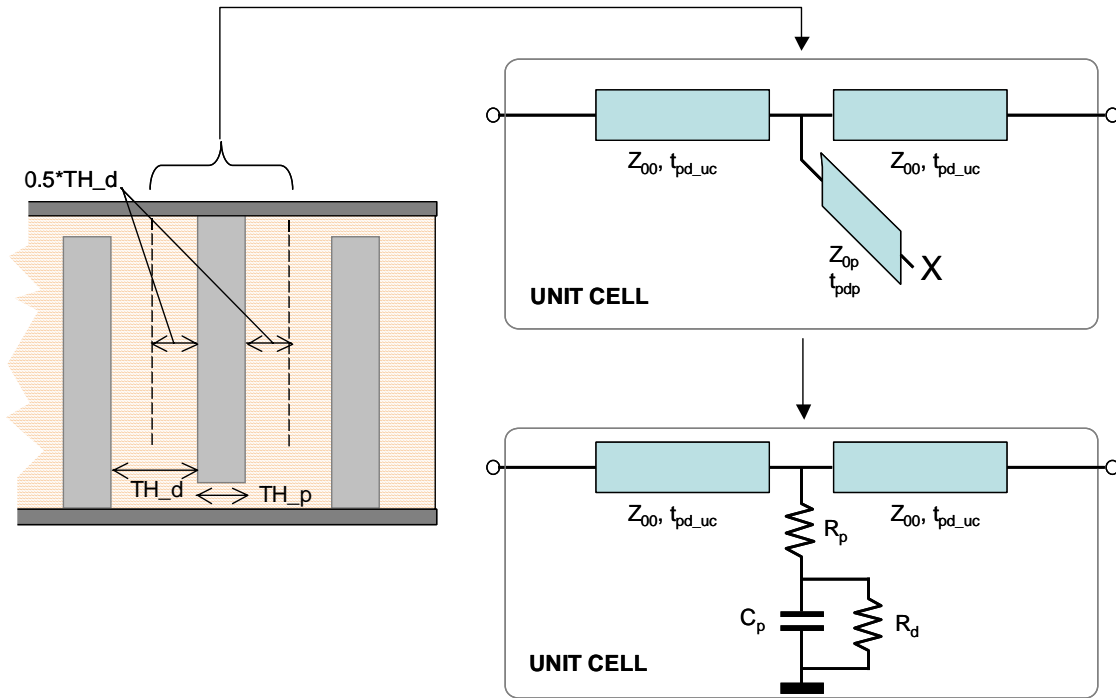


Figure 9. Generating unit-cell parameters from the geometry.

In (12), we can substitute the appropriate capacitance and loss-tangent values for the unloaded transmission line of terminals or the lossy transmission line of capacitor plates.

This generic model links the geometry and material properties of an MLCC to a causal electrical model, which can be directly used to calculate the impedance of the capacitor. Though this model is still too complex to include in an actual circuit simulator in multiples of copies, it is very suitable for correlation purposes. We can use any of the computer math packages to obtain the input impedance of the periodically loaded transmission-line circuit, which represents the impedance of the capacitor.

The lossy transmission-line model

The model derived in Figures 7 through 9 is generic, and as such, it is valid over a wide range of parameters. When we look at the actual geometry and resulting model numbers for a typical MLCC, we can achieve substantial simplifications without major loss of accuracy.

Since we are interested in the input impedance of the structure with open at its end (on the top), the second end piece of unloaded transmission line can be totally neglected. Because it is open terminated on the right, only the static capacitance of the end piece would matter anyway. Not having capacitor plates in the end piece, for large N, its static capacitance is orders of magnitudes lower than the total capacitance, and therefore it can be rightfully ignored.

The end piece on the left is in series to the external connections, and therefore cannot be completely ignored. We can still, however, simplify the left end piece by using the earlier arguments, and neglect its parallel capacitance and conductance. This leaves us with its series inductance and resistance. These values can be obtained from (3) and (4), by substituting H1 for H.

$$L_{0_end} = \mu_0 \frac{H1 * W}{L} \quad (13)$$

$$R_{t_end} = \frac{1}{\sigma_t} \frac{H1}{L * TH_t} \quad (14)$$

The unit cells can be simplified in a similar way. Capacitances and conductance of the series unloaded transmission-line pieces can be ignored, leaving only a series L-R term. For one unit cell, using the suffix *uc*, and substituting $TH_p + TH_d$ for H1, we get:

$$L_{0_uc} = \mu_0 \frac{(TH_p + TH_d) * W}{L} \quad (15)$$

$$R_{t_uc} = \frac{1}{\sigma_t} \frac{TH_p + TH_d}{L * TH_t} \quad (16)$$

The open-ended loading transmission line formed by adjacent capacitor plates can be simplified by neglecting its inductance. The Cp capacitance and Rp series resistance of the transmission line were already given in (6) and (9). There is one more element though that we don't want to ignore: the parallel conductance of the loading open-ended transmission line. It can be calculated from (12), by substituting the values for one plate pair:

$$G_p = 2\pi f C_p \tan \delta \quad (17)$$

These simplifications lead to the equivalent circuit of the unit cell shown in Figure 10. The shunt capacitance has its own Gp conductive loss term originated from the dielectric loss tangent, and an Rp series resistive loss term originated from the resistance of the adjacent capacitor plates. At any given frequency, the series and parallel loss terms can be combined into a single term. The schematics on the right of Figure 10 shows a parallel equivalent, where G'p represents a combination of Rp and Gp.

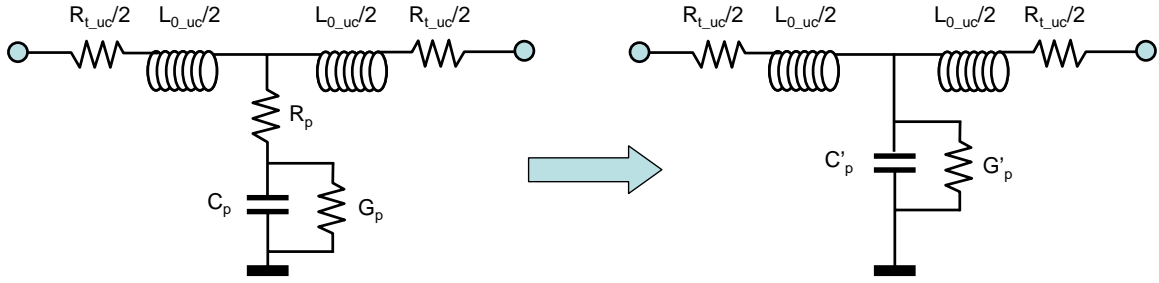


Figure 10. Equivalent schematics of the simplified unit cell. We get the circuit on the left by neglecting the capacitance and conductance of the series transmission line and by neglecting the inductance of the parallel transmission line. We get the circuit on the right by combining the series and parallel loss terms around the shunt capacitance.

Note that during the transformation, in a general case, both the capacitance and conductance will change. Assuming that \tan_{δ} is small, we get:

$$C'_p = \frac{C_p}{1 + \left(\frac{\omega}{\omega_p}\right)^2} \quad \text{and} \quad G'_p = G_p + \omega C_p \frac{\omega}{\omega_p} \quad (18)$$

If $\tau_p \ll 1$, the formulas can be further simplified to:

$$C'_p \approx C_p \quad \text{and} \quad G'_p \approx G_p + \omega C_p \frac{\omega}{\omega_p} \quad (19)$$

By combining (17) and (19), we get:

$$G'_p = \omega C'_p \tan_{\delta} + \omega C'_p \omega \tau_p \quad (19)$$

From (19) and (12) we can calculate a virtual loss tangent for the lossy transmission line:

$$\tan_{\delta}' = \frac{\tan_{\delta} + \frac{\omega}{\omega_p}}{1 + \left(\frac{\omega}{\omega_p}\right)^2} \quad (20)$$

In the final step we can realize that the cascaded unit cells represent the ladder equivalent of a uniform lossy transmission line. To obtain the per-unit-length transmission-line equivalent parameters, we multiply the unit-cell parameters by N . The inductance and the resistance are then simply the inductance and resistance of the (H-2*H1) section of the vertical terminals. The capacitance will become approximately the full capacitance of the part itself, though as indicated by (18), it drops sharply above the ω_p corner frequency. Moreover, to obey causality, the capacitance also drops slightly with frequency due to the finite loss tangent. The parallel conductance can be calculated from the full capacitance and the virtual loss tangent.

This eventually leads us to the simplified equivalent circuit of Figure 11. Note that this simple circuit is causal, and works on many time-domain and frequency-domain simulators.

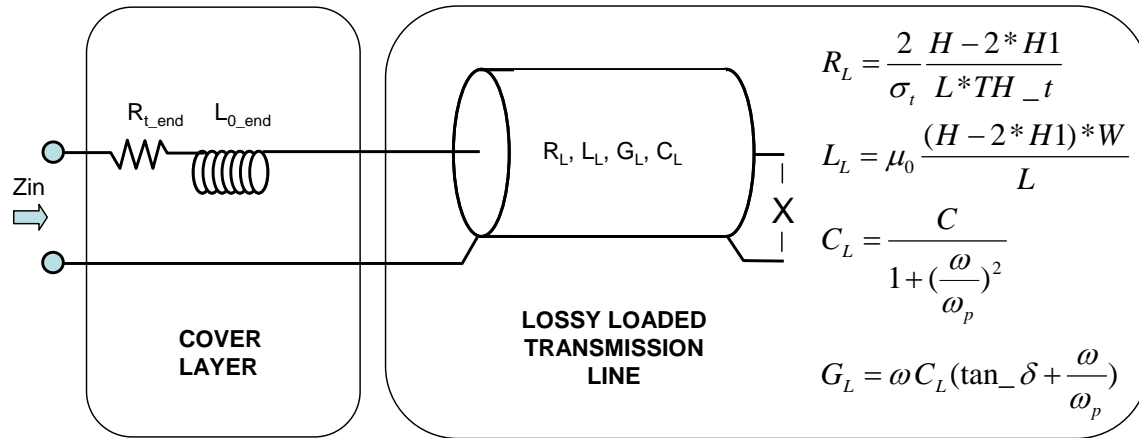


Figure 11. Simplified causal equivalent circuit of a Multi-Layer Ceramic Capacitor.

Note that the important aspect of this simplified model is not the lossy transmission line itself, rather the unique way that it captures the convoluted effect of conductive and dielectric losses in the frequency dependent capacitance and conductance per unit length.

III. Correlations

Characterization of test fixture

Now we return to the example shown in Figure 3. The 10uF 0508 MLCC part was measured in a small fixture, shown in Figure 12. The fixture has 22 layers. Capacitor sites are on top and bottom, connecting to 400x600 mil rectangular plane shapes further down in the stack. The horizontal layout of the site used for this test is shown on the right of Figure 12. The capacitor pads for the 0508 site are on the bottom side (layer 22), connecting to power planes on layers 20 and 21 with a set of blind vias.

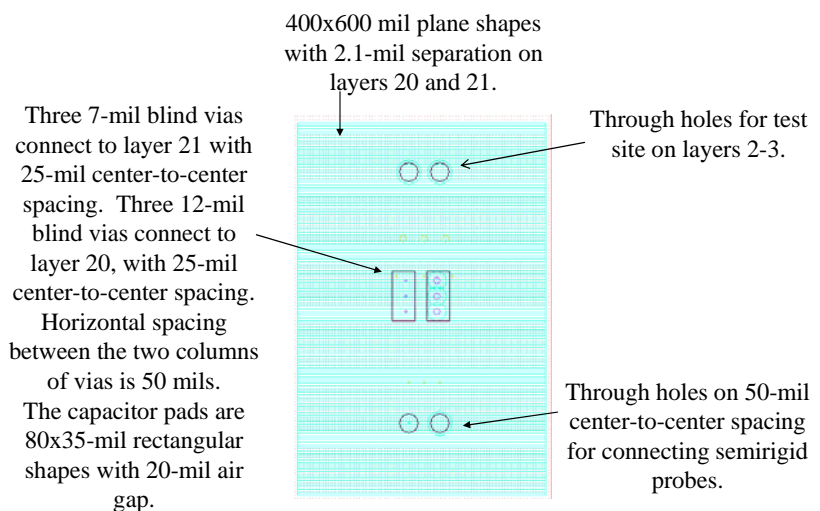
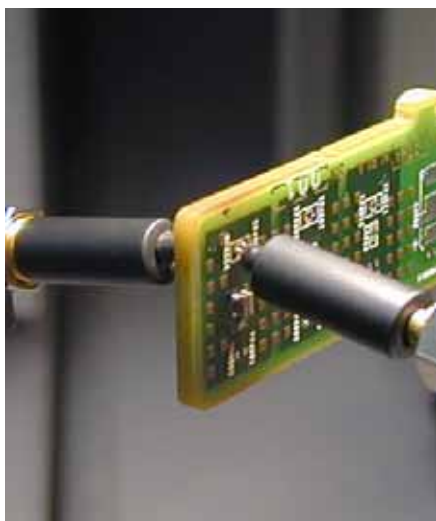


Figure 12. Geometry of test fixture for measuring the 10uF 0508 MLCC sample.

First the test site was characterized with the capacitor pads open and shorted with two Vector Network Analyzers (VNA): 4395A in the 100Hz – 10MHz frequency range and 4396A in the 100kHz to 1800MHz frequency range. Figure 13 shows the measured impedance magnitude and phase of the open test site and the extracted capacitance versus frequency. Note the straight slope of the capacitance curve on the linear-logarithmic scale; this indicates an approximately 2% of loss tangent of the FR4 material. The average capacitance is around 120pF at 10MHz.

Figure 14 shows the measured data and extracted parameters with the capacitor pads shorted. The graphs show composite data from both VNAs. The blue line on the left graph is the measured real part of the impedance; the green line is an approximation curve. The blue line on the right graph is the inductance extracted from the imaginary part of the measured impedance. The green line is a curve approximating the extracted inductance. The expressions approximating the real part and inductance:

$$R(f) = R_{DC} \left(1 + \left(\frac{f}{f_R}\right)^N\right) \quad \text{and} \quad L(f) = L_{inf} + \frac{\Delta L}{1 + \left(\frac{f}{f_R}\right)^N} \quad (21)$$

Where $R_{DC} = 1.7E-3$ [ohm], $f_R = 1.2E7$ [Hz], $L_{inf} = 1.4E-10$ [H], $\Delta L = 8E-11$ [H], $N = 0.8$.

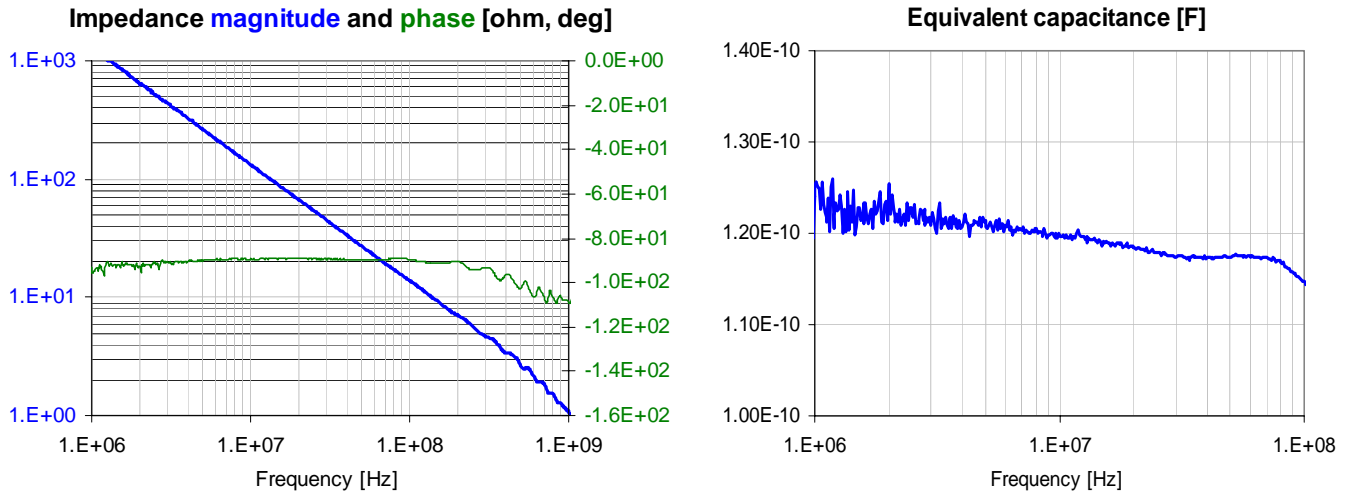


Figure 13. Left: impedance magnitude and phase measured on the test site with open pads. Right: extracted capacitance of the test site versus frequency.

The parallel capacitance of the open test site and the series resistance and inductance of the shorted test site have to be included when we are looking for correlation of the lossy transmission-line capacitor model to measured data. Note, however, that the shorted test site data also reflects resistance and inductance of the short itself, not only the test fixture. Since the short later is replaced with the capacitor, this small part of resistance and inductance will be double counted.

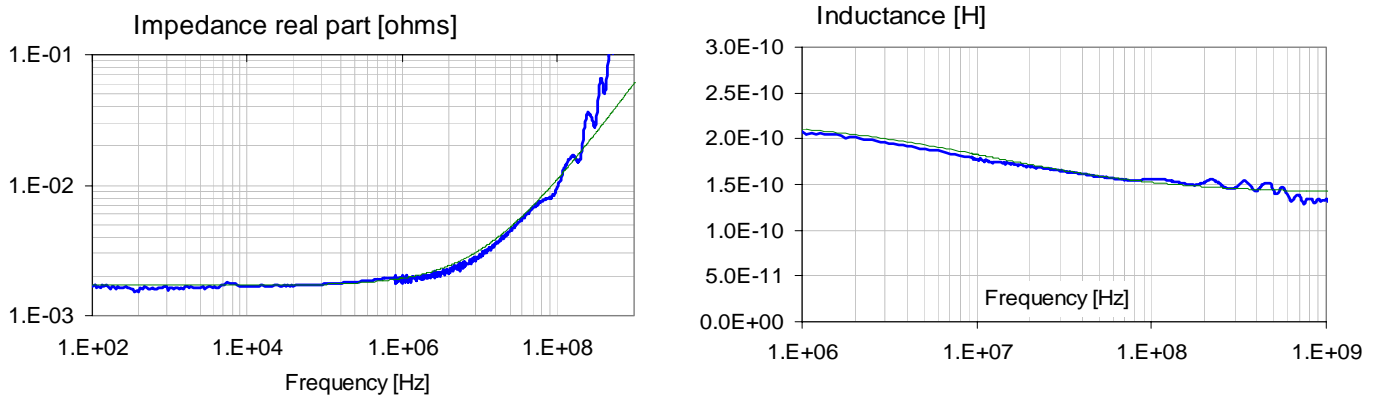


Figure 14. Impedance real part and extracted inductance of the shorted test site. Blue lines are measured data. Green lines are approximating curves based on (21).

Checking the convergence of unit-cell model

The unit-cell model captures the physical properties of the capacitor, and converts them into an electrical model. Strictly speaking we would need to know how many capacitor plates the part has, and concatenate the same number of unit cells. On the other hand, many times we do not know the number of capacitor plates in the part. And, clearly it is not even necessary. The per-unit electrical parameters of concatenated unit cells saturate beyond a number, resulting in diminishing change as we add more cells. The saturation curve does depend somewhat on the characteristics of the unit cell, but usually 50-100 cells will result in a sufficiently accurate approximation. Figure 15 illustrates the convergence with the unit cells used to describe the capacitor sample in Figure 3. For this exercise, the unit cells have been readjusted so that the given number of unit cells always added up to the same fixed characteristics of the sample capacitor.

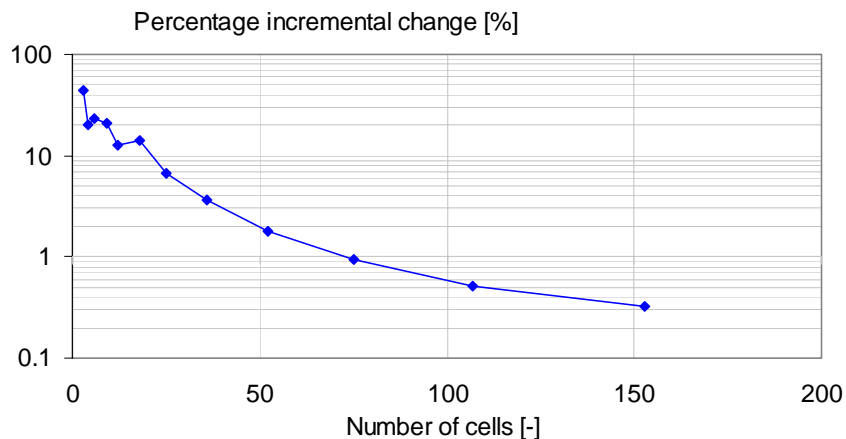


Figure 15. Saturation curve of concatenated unit cells. Vertical axis: percentage change between consecutive iteration with different number of unit cells. Horizontal scale: number of unit cells.

Correlation with unit-cell model

As opposed to the capacitance curve of the FR4 material of the test fixture, the extracted capacitance versus frequency on the right-hand graph of Figure 3 exhibits multiple sections of frequency ranges with approximately constant slope. This behavior suggests that for each of these frequency ranges a different dielectric loss tangent should be applied. This is illustrated in Figure 16, where we compare the correlations with a single dielectric loss tangent value (0.015) versus three different loss tangent values (0.025, 0.0135, 0.01). With three loss tangent values, applied separately for each frequency range, and combined linearly to continue to enforce causality, we can properly capture the shape of the impedance real part (and also the frequency dependency of the capacitance) over three decades of frequencies.

Below the Series Resonance Frequency (SRF) the capacitance and impedance real part are primarily coming from the dielectric material, and therefore the extracted capacitance versus frequency curve gives useful guidance how many segments we may need to use to properly describe the frequency dependency of the dielectric material. Near to and above SRF, on the other hand, we have no direct indication about the possible change of the loss tangent. We can, for instance, assume that the loss tangent just below SRF continues unchanged above SRF as well. This approach was followed in the correlation results shown here. As an alternative solution, we can assume additional frequency segments above SRF with their respective and unknown loss tangent values, and get the values by optimized curve fitting to measured data.

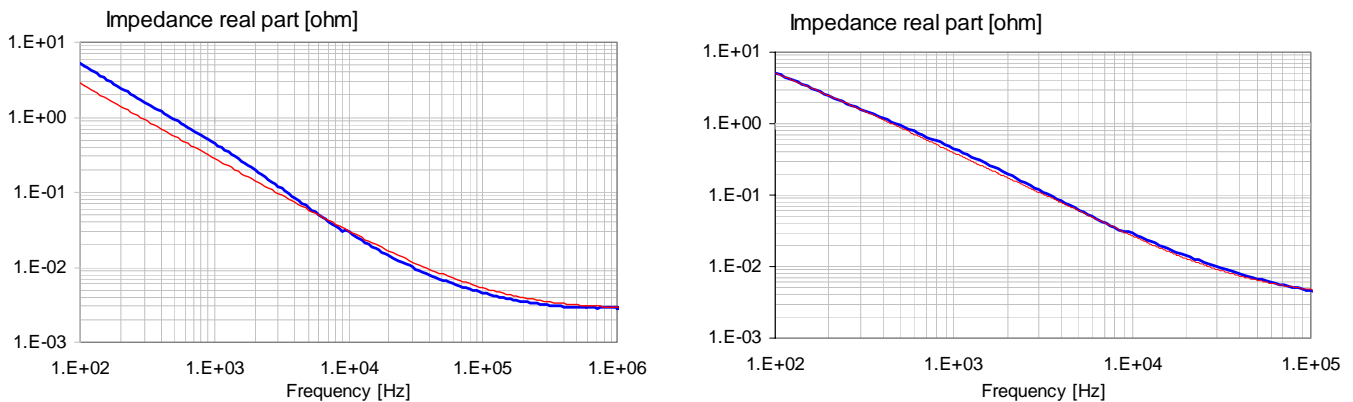


Figure 16. Correlation of impedance real part below the series resonance frequency. Measured: blue lines. Approximation: red lines. On the left: approximation using one loss tangent value. On the right: approximation using three different dielectric loss tangent values.

Once we have the capacitor parameters below SRF, we can put together the full model: cascaded unit cells, end piece, fixture. These models are based on the physical parameters of the capacitor. In this case, however, the measured part was not cross sectioned, and the internal geometry and material constant data was not available from other sources either. The correlation was, instead, done by manual and automated optimization of the model, with seed values based on reasonable assumptions. The number of parameters to be optimized is large enough that a reasonable correlation should be possible to achieve. However, not having the true numbers for the capacitors, a very accurate correlation was not the goal at this time. Instead, different parameter settings have been tried to see if the model can properly describe and capture the important characteristics of the measured data plots: increased ESR at SRF, sudden increase of ESR above SRF, slow rise of ESR above the secondary resonances.

As an illustration, Figure 17 shows the correlation after a brief optimization.

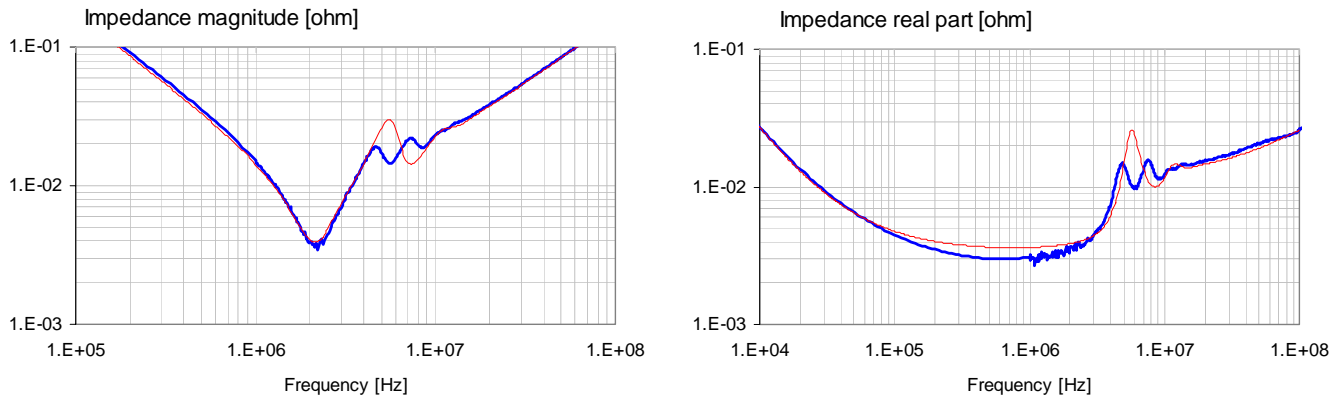


Figure 17. Correlation with unit-cell model. Measured: blue lines. Approximation: red lines.

Correlation with lossy transmission-line model

The same set of measured data was also correlated to the lossy transmission-line model. Figure 18 shows the correlation after a brief manual optimization of parameters.

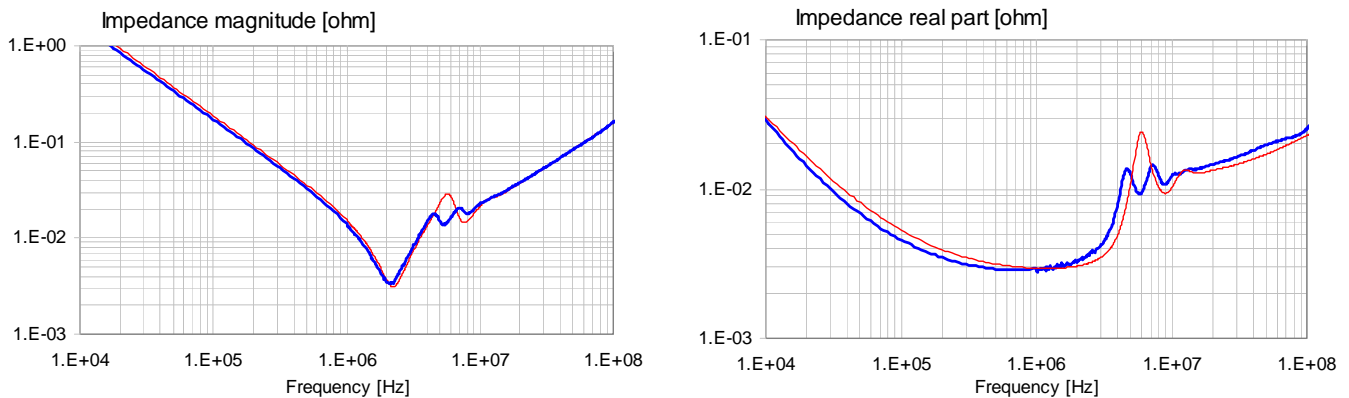


Figure 18. Correlation with lossy transmission-line model. Measured: blue lines. Approximation: red lines.

Conclusions and future work

It was shown that a causal model can be constructed for MLCC, which can capture the primary and secondary resonances of the part. The model is based on physical parameters of the capacitors, but the exact knowledge of these parameters is not a must: the parameters can be obtained by fitting the model to measured data. The parameters of cascaded unit cells can be combined into a single lossy, frequency and parameter-dependent transmission-line equivalent circuit. The simplified model is suitable many frequency and time-domain simulators, and simple enough to be used in multiple copies in Power Distribution Network simulations. Future work will examine correlation to parts with known internal geometry.

References

- [1] Istvan Novak, Jason R. Miller, "Frequency-dependent characterization of bulk and ceramic bypass capacitors," Proceedings of EPEP2003, October 27-29, 2003, Princeton, NJ.
- [2] A. Djordjevic, et al., "Wideband Frequency-Domain Characterization of FR-4 and Time-Domain Causality," IEEE. Tr. EMC, Nov. 2001, p.662.
- [3] Michael J. Hill, Leigh Wojewoda, "Capacitor Parameter Extraction – Techniques and Challenges," Intel Technology Symposium, Fall 2003.
- [4] Larry Smith, "MLC Capacitor Parameters for Accurate Simulation Model," in TF7 "Inductance of Bypass Capacitors; How to Define, How to Measure, How to Simulate" Proceedings of DesignCon 2005, January 31 – February 3, 2005, Santa Clara, CA.
- [5] Istvan Novak, "Frequency-Domain Power-Distribution Measurements – An Overview," HP-TF1 TecForum, DesignCon East, June 23, 2003, Boston, MA.
- [6] Hideki Ishida, "Measurement Method of ESL in JEITA and Equivalent Circuit of Polymer Tantalum Capacitors," in TF7 "Inductance of Bypass Capacitors; How to Define, How to Measure, How to Simulate" Proceedings of DesignCon 2005, January 31 – February 3, 2005, Santa Clara, CA.
- [7] L.D.Smith, D.Hockanson, K.Kothari, "A Transmission-Line Model for Ceramic Capacitors for CAD Tools Based on Measured Parameters," Proc 52nd Electronic Components & Technology Conference, San Diego, CA., May 2002, pp.331-336.
- [8] Charles R. Sullivan and Yuqin Sun, "Physically-Based Distributed Models for Multi-Layer Ceramic Capacitors," Proceedings of EPEP2003, October 2003.
- [9] Istvan Novak, " A Black-Box Frequency Dependent Model of Capacitors for Frequency Domain Simulations," DesignCon East 2005, September 19-22, 2005, Worcester, MA.
- [10] http://home.att.net/~istvan.novak/papers/Grid_sweep.zip